Seismic fragility models for typical non-engineered URM residential buildings in Malawi

Nicola Giordano [a,*], Raffaele De Risi [a], Elia Voyagaki [a], Panos Kloukinas [b], Viviana Novelli [c], Innocent Kafodya [d], Ignasio Ngoma [d], Katsuichiro Goda [e], John Macdonald [a]

[a] Department of Civil Engineering, Queen's Building, University Walk, University of Bristol, BS8 1TR Bristol, UK
[b] Faculty of Engineering and Science, University of Greenwich, Medway Campus, P351 Pembroke Building, Chatham Maritime ME4 4TB, UK
[c] School of Engineering, Cardiff University, Queen's Buildings, The Parade, Cardiff CF24 3AA, UK
[d] Department of Civil Engineering, University of Malawi, The Polytechnic, Blantyre, Malawi
[e] Department of Earth Sciences, Western University, London N6A 5B7, Canada

ABSTRACT

Malawi is an earthquake-prone country that lies within the East African Rift. A large proportion of its population lives in non-engineered single-storey constructions made of clay bricks and low-strength mortar. Walls are typically single-skin and often lack adequate wall-to-wall connections, leaving them vulnerable to seismic actions. This work reports a comprehensive study on the seismic fragility of unreinforced masonry buildings of the Malawi housing stock. The probability of exceeding different levels of in-plane/out-of-plane damage is estimated by considering the aleatory and epistemic uncertainties of the problem. Inter-building and intra-building variability are accounted for by adopting material test results and building survey data collected in Malawi. The in-plane capacity of building walls is calculated through a finite element model that considers the orthotropic properties of masonry. The out-of-plane capacity is computed using an analytical solution, developed for walls in one way bending. In addition, record-to-record variability is considered. The new country-specific fragility models result more conservative that global estimates, which reflects the high vulnerability of Malawian masonry buildings. These fragilities can be integrated into catastrophe modelling platforms for earthquake risk assessment in Malawi and in the wider East African region.

1. Introduction

Malawi has one of the highest rates of population growth in the world. According to the United Nations [1], the total population will increase from 18.6 million in 2019 to 38.1 million by 2050. This trend will inevitably result in increased exposure to natural disasters, such as earthquakes and floods [2–4]. Additionally, owing to the unregulated and inadequately planned nature of urban growth in Malawi, informal settlements, typical of rural areas, will be expanded at the outskirts of major cities, such as Lilongwe and Blantyre [5]. Residential buildings are characterised by poor engineering and construction quality, and are therefore highly vulnerable to natural hazards [6]. The location of Malawi, spanning over the southern branch of the active East Africa Rift, makes the country susceptible to M_w7.0 (or even greater) earthquakes [7]. Moderate seismic hazard, high vulnerability, and increasing exposure are attracting the attention of international agencies towards the

implementation of Disaster Risk Reduction (DRR) actions in Malawi [8].

The urgency of developing risk-informed DRR policies comes with the need for tailored risk assessment models for the region. Only a few studies are currently available on the topic. In 2016, Goda et al. [7] presented a first-generation probabilistic seismic risk model for Malawi. The model was developed as a combination of recent findings in seismic hazard [9] and global models for exposure/vulnerability [10,11]. Regarding structural vulnerability, the study emphasised that the adoption of global empirical models [10,11] may lead to potential bias and significant variation in the prediction of collapse rates. Moreover, the classification of the Malawian building stock through global building classes can be rather subjective and consequently uncertain and questionable [12]. More recently, the Global Earthquake Model (GEM) Foundation has released a new set of models for seismic risk assessment, including a global fragility/vulnerability database [13], a global hazard model [14], and an exposure database for different geographical regions, including East Africa [15]. According to GEM

Fig. 1. (a) Typical single storey Malawian brick-in-cement masonry building, (b) typical roof made of light timber truss supporting corrugated metallic corrugated sheet light-weight roof. Pictures source: Novelli et al., World Housing Encyclopedia, Report #205 [18].

estimates, the average annual loss of the residential building stock of Malawi is USD 10.3 million, roughly 0.025% of the total asset replacement cost. This estimate can be further improved by reducing the uncertainties around the current hazard data and by incorporating country-specific vulnerability models.

Consulting with the technical-scientific literature, it is clear that Malawi, when compared with other seismic-prone nations, lacks country-specific vulnerability/fragility models for earthquake risk assessment. Only recently, Novelli et al. [16] have proposed a first set of analytical fragilities for non-engineered constructions in Malawi. The work (i) presents the geometry of 646 façades of 327 houses, classified by structural features and potential failure modes and (ii) derives fragility curves by adopting the FaMIVE (Failure Mechanism Identification and Vulnerability Evaluation) mechanical approach [17]. Building on this previous research, the objective of this work is to enrich the current portfolio of fragility curves for the country focusing on informal, non-engineered, unreinforced masonry (URM) residential buildings (Fig. 1). In particular, by referring to the classification of Kloukinas et al. [12], URMs with the following characteristics are considered ("UFB*" in [12]): (i) fired bricks in cement mortar assemblage, (ii) absence of timber/concrete lintels, (iii) light metal roof (no diaphragm action), (iv) rectangular plan shape, and (v) single storey.

In order to derive fragility curves representative of actual URM residential buildings in the country, the analysis is carried out by considering the database reported by Novelli et al. [16], that includes information of houses located in different areas of the country, as shown in Fig. 2a. The dataset contains the geometric data of the surveyed houses that defines the inter-building variability of the construction class. Fig. 2b-c shows histograms of the façades' heights and thicknesses, indicating that the geometrical characteristics of the façades are highly variable. Additionally, a set of experimental tests on local masonry [19,20] is used to characterise the mechanical properties in a statistical manner.

The methodology adopted to derive seismic fragilities consists of two parts: (i) an In–Plane (IP) damage assessment is carried out by analysing each façade with a nonlinear orthotropic Finite Element (FE) model that accounts for the regularity (stretcher bond) of the masonry assemblage; (ii) an Out-Of-Plane (OOP) damage assessment is executed on each façade through an analytical closed-form procedure developed by Giordano et al. [21]. Both assessments start with the estimation of the nonlinear static capacity curve (*pushover*) of the façade. Subsequently, the amplitude of the seismic Intensity Measure (IM) that triggers a specific Damage State (DS) is calculated by adopting two procedures from the literature: SPO2IDA (Static Pushover to Incremental Dynamic Analysis) by Vamvatsikos and Cornell [22] and a CSM-based procedure (Capacity Spectrum Method [23]) proposed by Lagomarsino [24] and adapted by Giordano et al. [25]. The final fragility curves are calculated by combining the assessments from the two methods on each façade in a consistent probabilistic manner. Section 2 presents the fragility assessment methodology of this study. Section 3

discusses the experimental response of typical Malawian masonry and presents a probabilistic model to be used for fragility derivation. Lastly, Section 4 discusses the fragility results with reference to existing studies from the literature and underlines the relevance of this work towards the implementation of country-specific seismic risk assessment analyses for Malawi.

2. Fragility assessment methodology

Malawian non-engineered URM buildings are characterised by several structural weaknesses that affect their seismic behaviour [16]. Consequently, the fragility assessment procedure should reflect these deficiencies by introducing suitable considerations in the analyses [25]. Given the lack of adequate wall-to-wall/wall-to-roof connections and the absence of box-behaviour due to flexibility of the roof [8], this study considers two main assumptions: (i) the building's fragility is governed by the fragility of its constituting façades (e.g. [25–27]), and (ii) the IP and OOP damage assessment of URM façades can be decoupled (e.g. [28,29]). The fragility methodology is schematically depicted in Fig. 3 and described in the following list.

a) *Stochastic generation of typological buildings* (Fig. 3a)

The first step of the methodology consists of generating an ensemble of buildings that reasonably represents the UFB* housing stock in Malawi. 646 façade geometries are extracted from the 327 buildings of the database in Fig. 2 (normally one façade for the short direction of the building and one façade for the perpendicular long direction) [16]. This represents the geometrical aleatory variability. For each façade, a set of URM material properties is assigned in a probabilistic manner. In particular, façades that belong to the same building are characterised by different mechanical parameters to take into account the variability of construction quality within the same construction [12]. The probabilistic distributions from which the random properties are extracted are based on experimental tests of local URM materials [19], as discussed in Section 3. This reflects the material aleatory variability.

b) *IP and OOP capacity of façades* (Fig. 3b)

The damage assessment of each façade is carried out by considering the IP and OOP nonlinear static (*pushover*) responses. The IP capacity is estimated with an FE analysis of the façade carried out in OpenSees [30] through STKO (Scientific ToolKit for OpenSees) [31]. To account for the non-symmetric response of irregular façades, the IP *pushover* is estimated for both positive and negative directions of the seismic forces. The OOP capacity is quantified with an analytical mechanics-based closed-form procedure developed by Giordano et al. [21]. The numerical-IP and analytical-

(a)

(b)

(c)
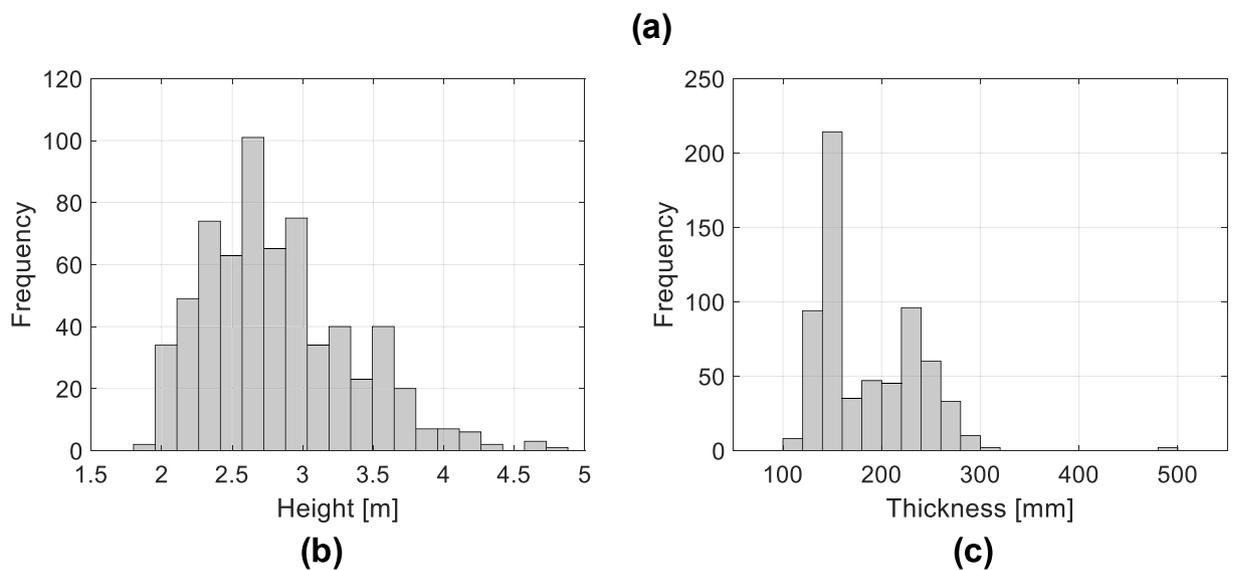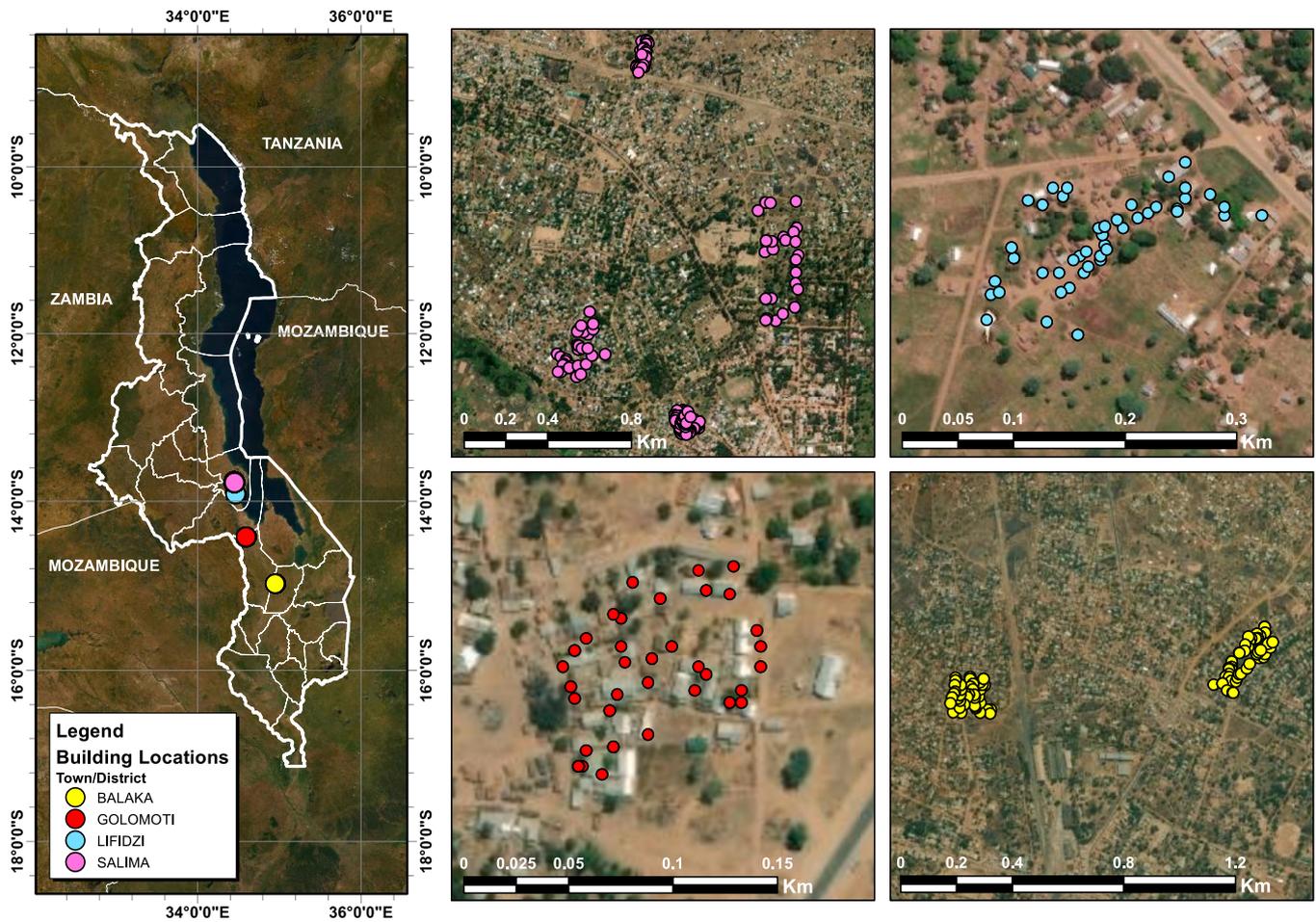
Fig. 2. (a) Geographical representation of the database of the surveyed buildings, (b) histogram of façade heights (average 2.82 m, coefficient of variation 18%), (c) histogram of façade thicknesses (average 183 mm, coefficient of variation 27%).

OOP capacity curves are then represented by bilinear/multi-linear models according to De Luca et al. [32]. Details of the IP/OOP capacity estimations are reported in Sections 2.1 and 2.2.

c) *Fragility curves of façades* (Fig. 3c)

For each façade's *pushover* diagram, a set of DS fragilities is generated by

adopting two methodologies: SPO2IDA [22] (described in Section 2.3.1) and CSM [23–25] (reported in Section 2.3.2). According to these techniques, the DSs are defined in terms of specific displacement thresholds on the *pushover* curve [13,33] (details in Section 2.3.3). The exceedance probability of a generic DS# is a function of a seismic IM. The IM selected for this study is the Peak Ground Acceleration (PGA). The adoption of the two assessment techniques (SPO2IDA/CSM) for each damage mode (IP/OOP) is

a fundamental step to characterise the epistemic uncertainty that each technique brings. As a result, every façade is defined by four sets of DS fragilities: (1) IP-SPO2IDA, (2) IP–CSM, (3) OOP-SPO2IDA and (4) OOP-CSM. It should be noted that for a given assessment technique, each façade is characterised by two sets of IP fragilities that correspond to *pushover* curves with positive and negative horizontal loads.

d) *Fragility curves of buildings & building class* (Fig. 3d)

The fragility sets of the façades are subsequently combined to obtain DS fragilities of each building. For a given damage mode (IP/OOP), DS#, and assessment technique (SPO2IDA/CSM), a building's DS# fragility corresponds to the maximum envelope of the DS# fragilities of its
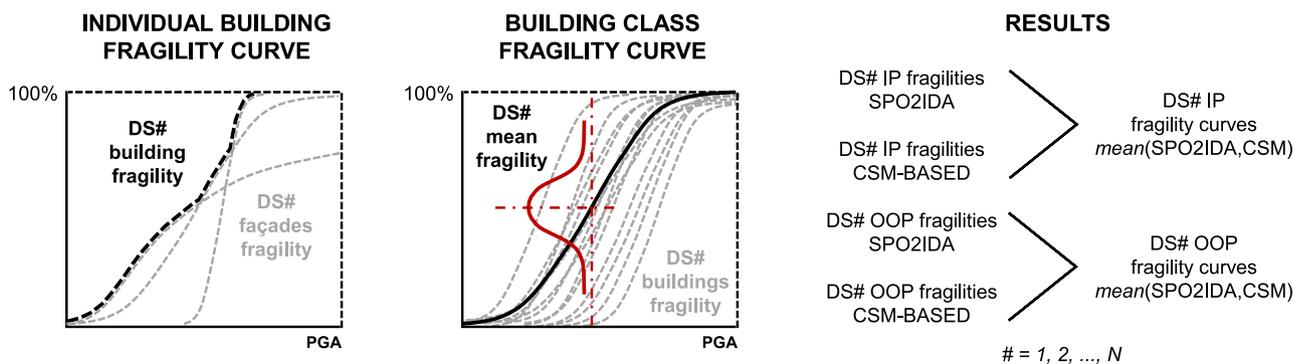
Fig. 3. Seismic fragility assessment methodology.

constituting façades (i.e. maximum probability of damage). Subsequently, the DS# fragility of the building class is calculated by averaging the fragility curves of all the buildings for each PGA. With the four sets of fragility curves listed in point (c) above, two final additional sets (IP and OOP) can be derived to account for the epistemic uncertainty of the assessment technique. For a given damage mode and a given PGA, the fragility curves of buildings derived with SPO2IDA and CSM are averaged to obtain a final fragility estimate (mean curve).

2.1. In-plane capacity

The IP capacity of a URM building can be estimated with a variety of methods that range from simplified analytical procedures to computationally expensive numerical techniques. Among the numerical approaches, many studies model buildings as FE equivalent frames, where the URM walls are discretised into a system of nonlinear piers, nonlinear spandrels, and rigid nodes [34,35]. The equivalent frame represents a reasonable simplification to assess the IP response of URMs and, owing to its low computational cost, can be used to perform probabilistic analyses (e.g. [36–38]). However, several studies have pointed out that the assumptions related to the frame discretisation are questionable [39], which increases the uncertainty of the assessment results [40]. An alternative to the equivalent frame is the Nonlinear Continuum FE (NC-FE) approach. It is usually implemented in two ways: by modelling masonry units and mortar joints with different constitutive models (micro-modelling), or by representing masonry as a single material with homogenised mechanical properties (macro-modelling) [41]. With this latter method, the different failure modes of masonry, such as cracking/crushing of units/joints and sliding of units are smeared out in a continuum [42,43]. Macro-modelling is generally preferred to the former since it requires less computational effort. There are various past studies on the experimental validation of NC-FE models (e.g. [42,44–46]), including results that are applied to historical URM buildings (e.g. [47–50]). In contrast, fragility assessment studies on URM building typologies based on NC-FE analyses are lacking in the literature. Two main reasons are the need for comprehensive information on URM mechanical parameters of the investigated structural typology (which are not usually available) and the computational cost of NC-FE models in performing a large number of seismic fragility analyses.

With the aims of executing NC-FE analyses and reducing the simplifications associated with IP modelling, the above-mentioned shortcomings are addressed in this work. The computational cost of NC-FE is reduced by using an implicit (at structure level) – explicit (at material level) nonlinear solver available in STKO [31,51] and implemented in OpenSees [30]. Additionally, taking advantage of available experimental results of Malawian masonry (Section 3), the URM orthotropic constitutive model is characterised in a probabilistic way. Specifically, each façade is discretised with quadrilateral plane-stress elements. Orthotropic material properties are assigned to the tension–compression plastic-damage model developed by Pelà et al. [43] and implemented in STKO [31,51]. Once the FEM model is built, nonlinear static *pushover* analysis is carried out by considering an inverse-triangular force distribution, as suggested by international codes [52].

2.1.1. Example of IP capacity of URM façade
An example of the procedure to identify the IP capacity is provided in Fig. 4. The selected façade is 2.4 m high, 3.6 m long, and 140 mm thick and is composed of two parts of different horizontal stiffness: a squat
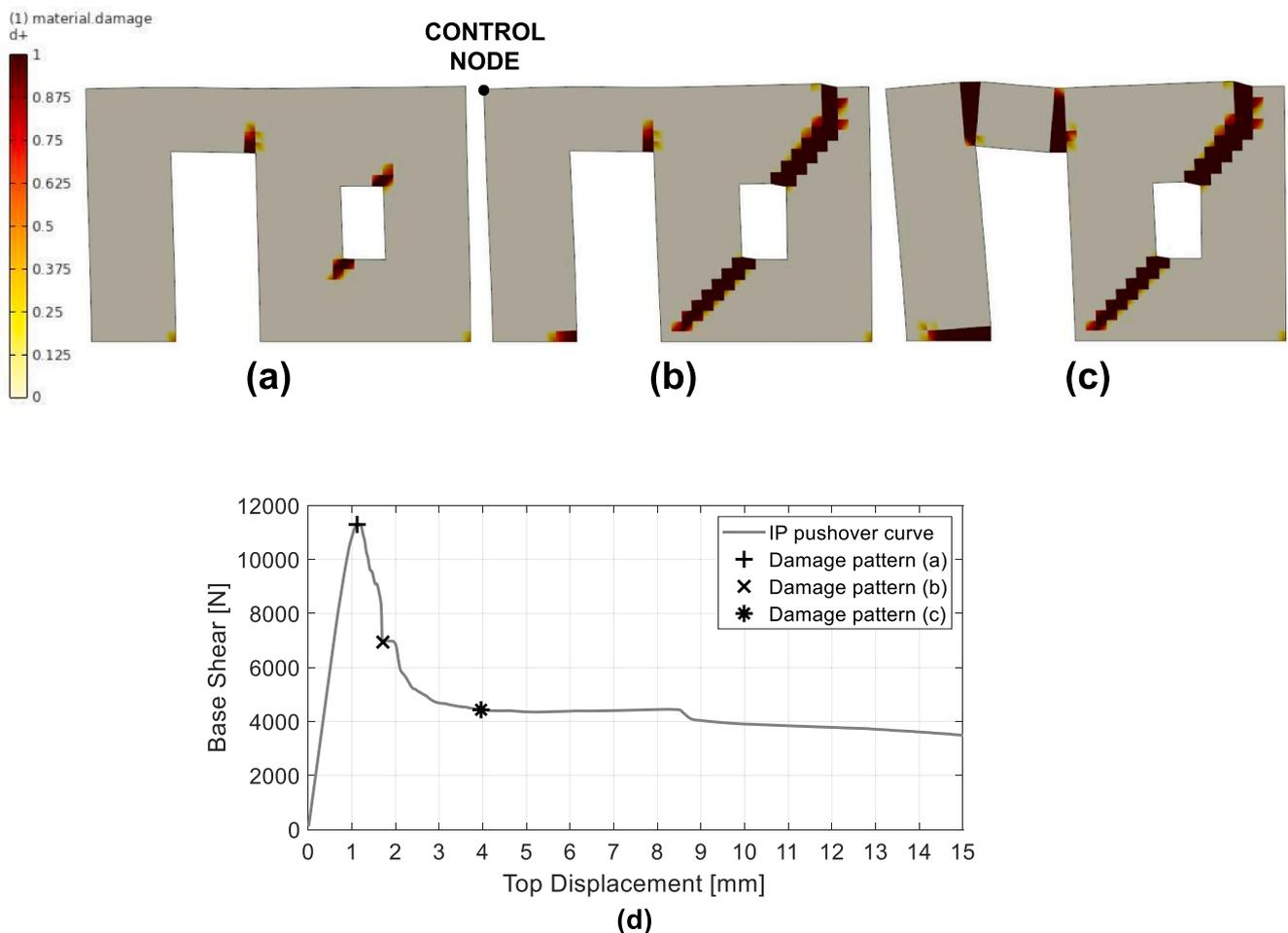
Fig. 4. IP numerical response of a representative façade where the contour plots show the material tensile damage (d +). (a) damage pattern at maximum horizontal capacity, (b) damage pattern at 61% post-peak capacity, (c) damage pattern at 39% post-peak capacity, (d) force-displacement diagram.

perforated wall (right side of the door) and a slender pier (left side of the door). The two portions are linked through a spandrel. The dimensions of the door and the window are 0.8 m × 1.8 m and 0.4 m × 0.7 m, respectively. The masonry mechanical properties are the median values of the distributions reported in Section 3.3. The mesh size of the quadrilateral elements is 100 mm × 100 mm. Fig. 4a-b-c show the damage patterns of the façade computed at different displacement levels for loading to the left, while Fig. 4d reports the force–displacement response of the façade. Fig. 4a corresponds to the maximum horizontal capacity (11.3 kN): cracks appear at the corners of the window and the bottom-right of the spandrel. Fig. 4b corresponds to a post-peak horizontal capacity equal to 61% of the maximum. A rocking mechanism of the top-left side of the perforated wall is activated. Subsequently, Fig. 4c shows an additional rocking mechanism of the left pier and consequent rotation of the spandrel. The corresponding horizontal capacity has decreased to 39% of the maximum capacity. These results highlight the complexity of the IP response of URM façades, especially in the absence of floor/roof constraints that prevent relative displacements of the top nodes. With such constraints, experimental quasi-static tests on URM façades have shown a very stable force–displacement response (e.g. [53,54]).

2.2. Out-of-plane capacity

The OOP capacity of the façades is quantified by adopting the analytical closed-form mechanical model developed by Giordano et al. [21] for the fragility assessment of traditional URM buildings in Nepal [25]. The method adopts three main assumptions: (i) as validated experimentally [55–59], the OOP capacity of a vertically spanning URM wall is governed by rocking; (ii) for the case of the cantilever configuration (i.e. with no constraint at the top of the wall), the wall is modelled as a rigid body connected to the ground with a nonlinear hinge; and (iii) the nonlinear response of the hinge is defined through the moment–curvature diagram of the base (critical) cross-section [60].

Utilizing the experimental data on OOP tests of Malawian URM that provide the tensile capacity of bed-joint interfaces, the cantilever model developed in [21] is improved by taking into account the tensile contribution of mortar joints in the initial-elastic phase. Fig. 5 depicts an example of an OOP *pushover* curve with reference to the façade of Section 2.1. The structure behaves in a linear elastic manner until the

maximum tensile strength of the base bed-joint is achieved (cracking). After the exceedance of the tensile strength, the façade behaves according to the nonlinear OOP response described by Giordano et al. [21].

2.3. Estimation of façade's fragility for a given DS#

As illustrated in Fig. 3c, for a given façade, the estimation of DS fragilities is carried out with SPO2IDA [22] and CSM [25]. In Sections 2.3.1. and 2.3.2, these approaches are described. As previously mentioned, the IM selected in this work is the PGA, since it is a reasonable measure for low-rise masonry buildings (e.g. [25,61,62]) and this information is available from national seismic hazard maps (e.g. [7,9]). In line with previous studies (e.g. [25,37,38]), DSs are defined as displacement thresholds on the *pushover* curve of the building. Section 2.3.3 reports the definition of DS limits with reference to IP and OOP responses.

2.3.1. SPO2IDA assessment

The first step of the SPO2IDA assessment is to convert the force–displacement *pushover* curve into a spectral-acceleration (S_a) versus spectral-displacement (S_d) capacity curve through the single degree of freedom (SDOF) equivalence (e.g. Eurocode 8 [52]). Subsequently, a simplified multi-linear model of the capacity curve is calculated according to De Luca et al. [32]. The multi-linear curve is then converted into a set of equivalent Incremental Dynamic Analysis (IDA) curves by adopting SPO2IDA [22]. Three curves, representing the 16th, 50th, and 84th percentiles of equivalent IDAs, are quantified to reflect the record-to-record variability. Given a DS# displacement threshold on the multi-linear capacity curve, the corresponding damage fragility is estimated by considering a lognormal distribution model. The median value $S_{a,50\%}$ corresponds to the 50th percentile estimate of the IDA. The dispersion is defined as $\beta = 0.5 \times \ln(S_{a,84\%}/S_{a,16\%})$. The resulting fragility is expressed in spectral–acceleration for the equivalent vibration period of the SDOF, T_{eq}. This period is directly calculated from the multilinear model. For instance, it has an IP average value of 0.065 s (CoV = 0.36) over the database of façades. To increase the practical usability of the fragility curves, the spectral-acceleration values are converted to PGA through a scaling relationship based on the Ground Motion Prediction Equation (GMPE) by Boore et al. [63]. This GMPE is suitable for shallow
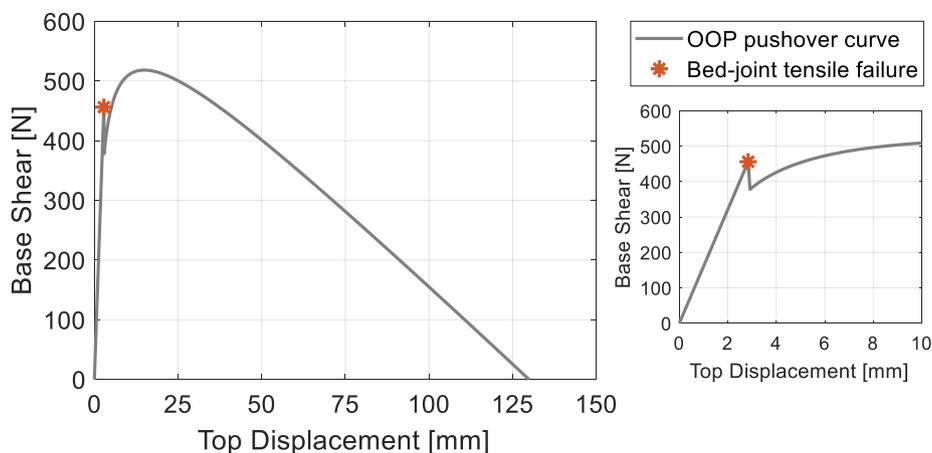
Fig. 5. Simulated OOP response of a representative façade. The star represents the cracking limit for tensile failure of the base bed-joint.

crustal earthquakes in active tectonic regions and it is based on global data. The conversion from $S_a(T_{eq})$ to PGA is carried out with Equation (1):

$$PGA = S_a(T_{eq}) \frac{\widehat{PGA}_{GMPE}}{S_a\widehat{(T_{eq})}_{GMPE}} \tag{1}$$

where $\widehat{PGA}_{GMPE}$ and $S_a\widehat{(T_{eq})}_{GMPE}$ are the average PGA and $S_a(T_{eq})$, respectively, from the GMPE, considering the case of normal faulting, top 30 m average shear wave velocity of 300 m/s [64], distance interval of 1 km to 30 km and magnitude interval of 5 Mw to 8 Mw [7,9]. Fig. 6a shows the described procedure for a generic DS#.

2.3.2. CSM assessment

The CSM assessment is carried out in reference to Giordano et al. [25]. In analogy with SPO2IDA, the force–displacement *pushover* curve is firstly mapped into the $S_a - S_d$ plane. Subsequently, for the sole IP capacity curve, a simplified bilinear model is calculated using the procedure presented by De Luca et al. [32]. Given a DS# displacement on the capacity curve, the following analysis steps are carried out to derive the corresponding fragility curve:

- 934 smoothed $S_a - S_d$ spectral shapes [65] from the SIMBAD (Selected Input Motions for displacement-Based Assessment and Design) database [66] are scaled to intersect the pushover curve at the DS# displacement, by using the CSM [21,23,24]. This results in a set of 934 PGAs.
- The 934 PGAs are sorted by their absolute scale factor, ASF = max {SF; 1/SF}, where the scale factor, SF, is the ratio between the scaled PGA (estimated with the CSM) and the PGA of the recorded ground motion [25]. Subsequently, the first (lowest ASF) 100 PGAs are selected. As discussed by Giordano et al. [25], this selection procedure preserves record-to-record variability while removing PGA values with excessively high scale factors [67].
- Lastly, the cumulative distribution of the 100 PGAs is fitted with a lognormal model to derive the DS# fragility.

Fig. 6b depicts the CSM assessment for a given façade and DS#.
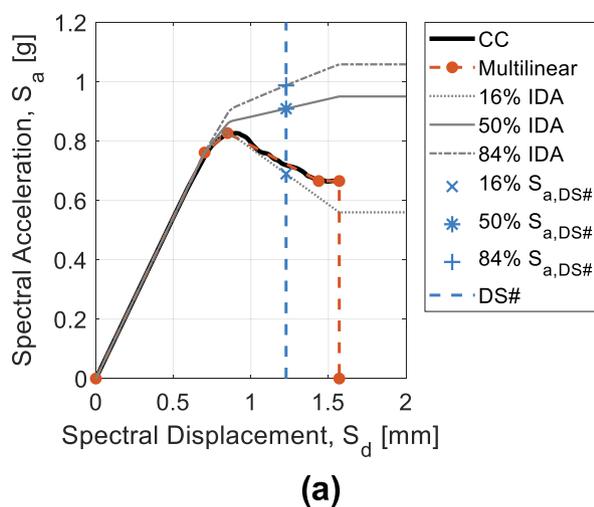
2.3.3. Definition of DSs

DSs are defined as displacement thresholds on the capacity curve. For the IP curve, the indications by Martins and Silva [13] are adopted:

- $S_{d,DS1}$ (*slight damage*) corresponds to 75% of the yielding displacement $S_{d,y}$ of the bilinear/multi-linear model;
- $S_{d,DS2}$ (*moderate damage*) is defined as $0.5 \times S_{d,y} + 0.33 \times S_{d,u}$, where $S_{d,u}$ is the ultimate displacement of the multi-linear/bilinear model. $S_{d,u}$ is defined on the numerical capacity curve as the displacement at 80% post-peak capacity;
- $S_{d,DS3}$ (*severe damage*) corresponds to $0.25 \times S_{d,y} + 0.67 \times S_{d,u}$;
- $S_{d,DS4}$ (*near collapse*) is equal to $S_{d,u}$.

OOP DSs are defined according to previous studies [13,25,33]:

- $S_{d,DS1}$ (*slight damage*) corresponds to the displacement at cracking ($S_{d,y}$), which is highlighted with a star in Fig. 5.
- $S_{d,DS2}$ (*moderate damage*) is defined as $0.5 \times S_{d,y} + 0.33 \times S_{d,u}$ [13];
- $S_{d,DS3}$ (*severe damage*) corresponds to 25% of the overturning displacement (i.e. displacement at null force) [25,33];
- $S_{d,DS4}$ (*near collapse*) is equal to $S_{d,u}$ and corresponds to 40% of the overturning displacement [25,33].

3. Probabilistic distributions of material properties

3.1. Experimental data of local materials

An extensive experimental programme was carried out in Malawi to characterise the mechanical properties of local masonry materials [19,20]. In this work, four sets of experimental tests are used to define the probabilistic material model of URM:

- *Vertical compression tests on masonry prisms* were carried out according to EN 1052-1 [68]. The prisms were each composed of five bricks having a nominal size of 200 mm × 90 mm × 50 mm. A total of twenty-four tests are considered in this study: (i) six tests characterised by a cement-to-sand ratio of 1:4 (the recommended value according to MS791-1 [69]) and realised in favourable (F) construction conditions (with clean and dampened bricks); (ii) six tests
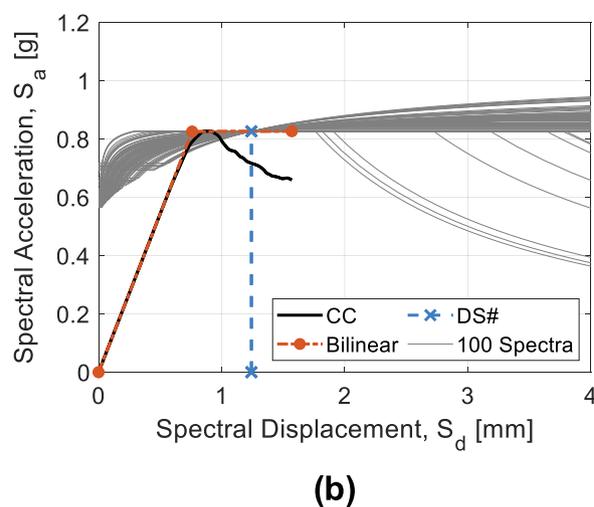
Fig. 6. (a) SPO2IDA assessment, (b) CSM assessment. 'CC' indicates the capacity curve of the façade.

with a cement-to-sand ratio of 1:4 and realised in unfavourable (U) conditions (bricks laid in a dry state and in the presence of dust); (iii) six tests characterised by a cement-to-sand ratio of 1:6 (minimum value indicated by the Safer House Construction Guidelines [70]) and realised in favourable conditions; and (iv) six tests with a cement-to-sand ratio of 1:6 and constructed in unfavourable conditions. The mechanical properties that can be obtained from the vertical compression tests are: the elastic modulus in the vertical direction (i.e. perpendicular to the bed-joints) (E_v), the compressive strength at the elastic limit in the vertical direction (f_{c0}), the ultimate compressive strength in the vertical direction (f_{cp}), and the corresponding strain in the vertical direction (ε_p). Fig. 7a-b shows the stress–strain results of the 1:4 and 1:6 tests, respectively. It is observed that the material behaviour varies significantly in strength, stiffness, and strain capacity, which can only be reflected by using an advanced numerical modelling technique (Section 2.1). In addition, the construction conditions (F/U) do not consistently affect the stress–strain results for either 1:4 or 1:6 cement-to-sand ratios.

- *Diagonal compression tests on masonry panels* were carried out by using the in-situ testing procedure presented by Brignola et al. [71]. The dimension of the masonry panels was approximately 1060 mm × 1060 mm with a thickness of 90 mm (one-brick thick). A total of twelve experimental results are considered: (i) six texts characterised by a cement-to-sand ratio of 1:4 and favourable construction conditions; and (ii) six tests characterised by a cement-to-sand ratio of 1:6 and unfavourable construction conditions. The masonry properties extracted from the diagonal compression tests are the shear modulus (G) and the equivalent shear strength (τ_0). Fig. 8a-b shows the stress–strain results of the 1:4 and 1:6 tests, respectively. As expected, the 1:4 panels (Fig. 8a) are considerably stronger than the 1:6 panels, but, at the same time, more brittle.

- *Compression tests on bricks* were carried out according to the Malawian standard MS6 [72] to quantify their strength (f_b). In total, 54 test results are considered. The sample exhibits a quite low median value (4.32 MPa) and high dispersion (coefficient of variation ≈ 0.40) with respect to typical international benchmark values (e.g.
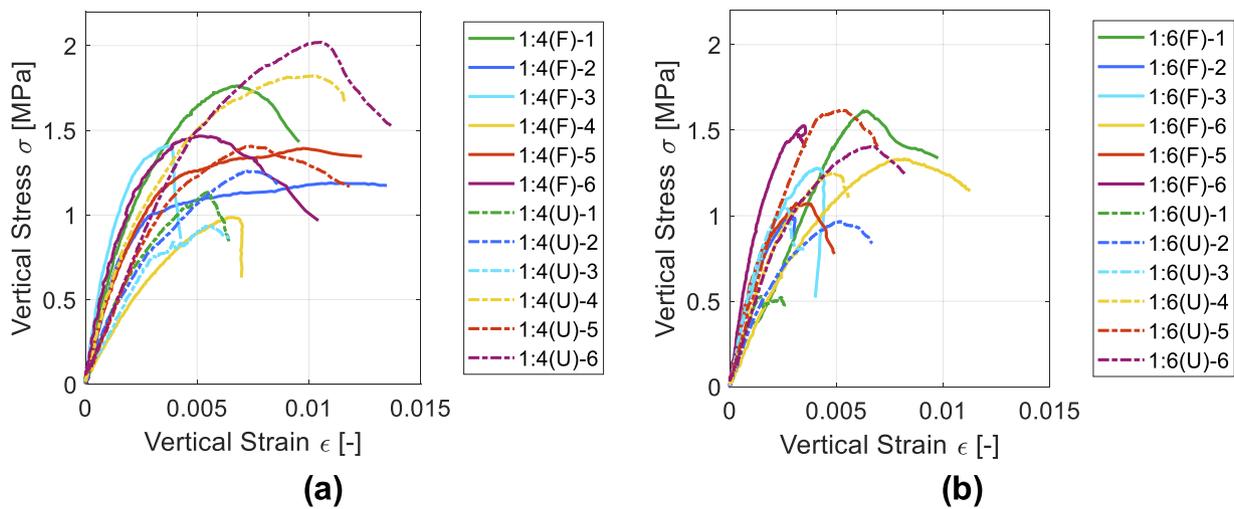
Fig. 7. Vertical compression tests on masonry prisms. Cement-to-sand ratio: (a) 1:4, (b) 1:6.
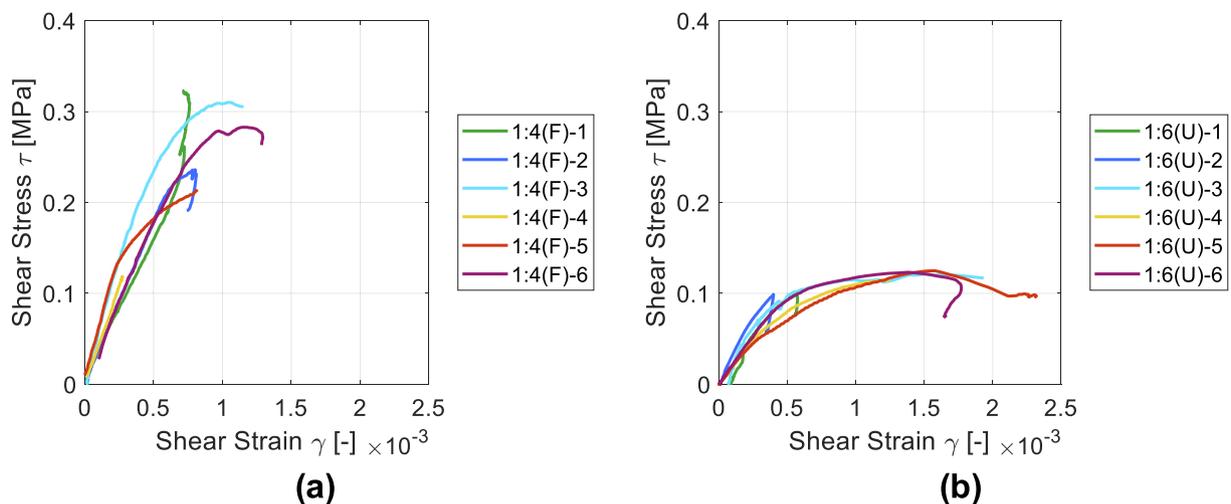
Fig. 8. Diagonal compression tests on masonry panels. Cement-to-sand ratio: (a) 1:4, (b) 1:6.

[73]), which is a consequence of the non-industrial production process of Malawian bricks.

- *OOP four point bending tests on masonry panels (bending parallel to the bed-joints)* were carried out according to EN 1052–2 [74]. The dimension of the URM specimens was 760 mm × 420 mm with thickness of 90 mm. A total of nine tests are considered where four of them are characterised by a 1:4 cement-to-sand ratio and favourable construction conditions, while five of them had a 1:6 cement-to-sand ratio and unfavourable construction conditions. In terms of mechanical parameters, the OOP bending tests provide the tensile strength of the mortar bed-joints ($f_{t,bj}$).

3.2. Numerical modelling of experimental tests

The experimental results reported in Section 3.1 are used as a benchmark for the calibration of the IP numerical analyses (Section 2.1). As previously discussed, given the periodic bond (stretcher bond) of typical Malawian brick masonry, the orthotropic material model by Pelà et al. [43] (*OrthotropicMaterial* in STKO [31]) is adopted. In addition to the mechanical parameters obtained from the tests (Section 3.1), additional parameters have to be defined for the orthotropic model. Therefore, the following assumptions are considered:

- The elastic modulus in the horizontal direction (parallel to the bed-joints), E_h, is quantified according to the formula that Mojsilovic [75] calibrated with 130 experimental compression tests on URM walls:

$$E_h = 3.5(1 + \nu)G - E_v \qquad (2)$$

were G can be assumed as 35% of E_v as in Wilding et al. [76]. Equation (2) is also consistent with the results of recent experimental investigations on URM panels tested in two orthogonal directions [77];

- The Poisson's ratio ν is assumed equal to 0.15 according to global data on masonry mechanical properties [78];

- The compressive strength of masonry in the horizontal direction is conservatively assumed as half of the value in the vertical direction to account for the weakness of head joints in low-quality masonry [8].

Fig. 9a shows a comparison between the results of a vertical compression test and a numerical simulation (test 1:4(F)-1). It is observed that the numerical model can accurately reproduce the experimental response of the prism. The average absolute error between experimental and numerical curves is 2.9%. The modelling of the full set of the tests provides an average absolute error between 2.4% and 9.7% (mean value: 5.6%). Fig. 9b shows a comparison between the results of a diagonal compression test and a numerical simulation (test 1:6(U)-6). In this case, the numerical model is less accurate in reproducing the experimental behaviour of the panel. This is the consequence of larger uncertainties in the modelling of diagonal compression tests with respect to vertical compression tests [71,79]. The experimental versus numerical comparison on test 1:6(U)-6 is characterised by an average absolute error of 9.0%. Additionally, looking at the full set of the tests, the average absolute error is between 4.6% and 17.3% (mean value: 10.3%).

3.3. Probabilistic models for masonry material properties

The mechanical properties extracted from the tests are used to define the URM material model in a probabilistic way. Each material property is represented by a lognormal distribution whose parameters (median and lognormal standard deviation) are reported in Table 1. Additional parameters required for conducting the IP numerical analyses are taken from the literature. Particularly, the fracture energy in compression (G_c) and in tension (G_t) are described with uniform probability distributions. The upper and lower limits of these distributions are taken from da Porto et al. [79]: $G_c = 5.0$ N/mm to 20.0 N/mm and $G_t = 0.018$ N/mm to 0.05 N/mm. It is worth mentioning that these intervals are consistent with the fracture energy values adopted for the numerical vs. experimental comparisons described in Section 3.2. Fig. 10a shows the probabilistic distributions of the main strength parameters, f_{c0}, f_{cp}, τ_0, and $f_{t,bj}$, while Fig. 10b shows the distributions of the stiffness parameters E_v, E_h, and G.
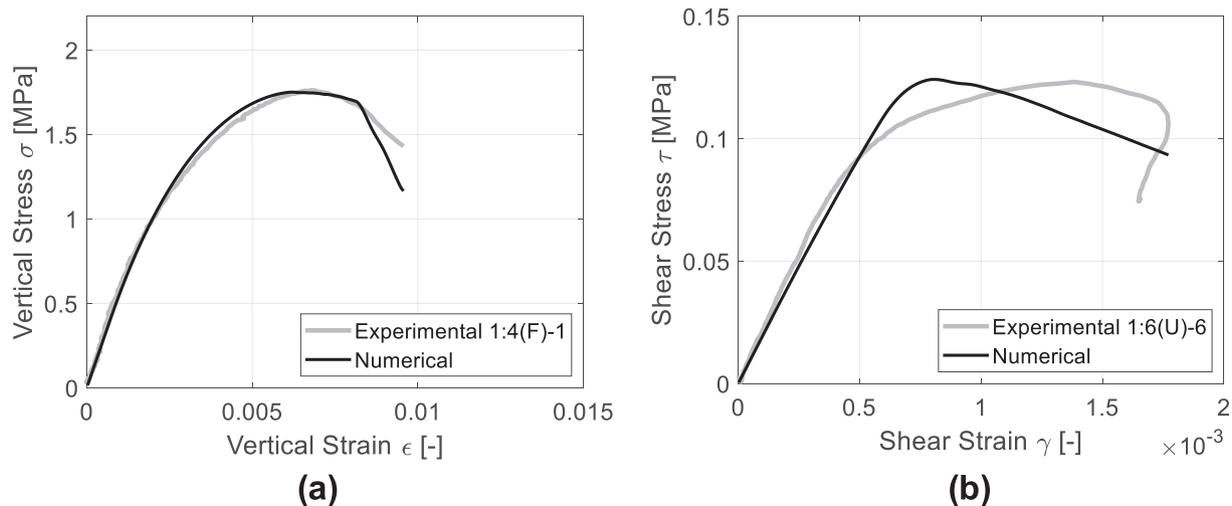
Fig. 9. Experimental versus numerical comparisons: (a) vertical compression test 1:4(F)-1, (b) diagonal compression test 1:6(U)-6.

Table 1
Probabilistic parameters of material properties extracted from the experimental tests.

Parameter	Description	Unit	Distribution Typology	Median	Lognormal Standard Deviation
E_v	*masonry elastic modulus(vertical)*	MPa	Lognormal	581.6	0.52
E_h	*masonry elastic modulus(horizontal)*	MPa	Lognormal	237.7	0.52
G	*masonry shear modulus*	MPa	Lognormal	203.5	0.52
f_b	*brick compressive strength*	MPa	Lognormal	4.32	0.42
f_{c0}	*masonry compressive strength at elastic limit*	MPa	Lognormal	0.53	0.35
f_{cp}	*masonry ultimate compressive strength*	MPa	Lognormal	1.27	0.28
ε_p	*masonry ultimate compressive strain*	–	Lognormal	0.0055	0.51
τ_0	*shear strength*	MPa	Lognormal	0.16	0.43
$f_{t,bj}$	*Tensile strength of bed-joints*	MPa	Lognormal	0.034	0.45
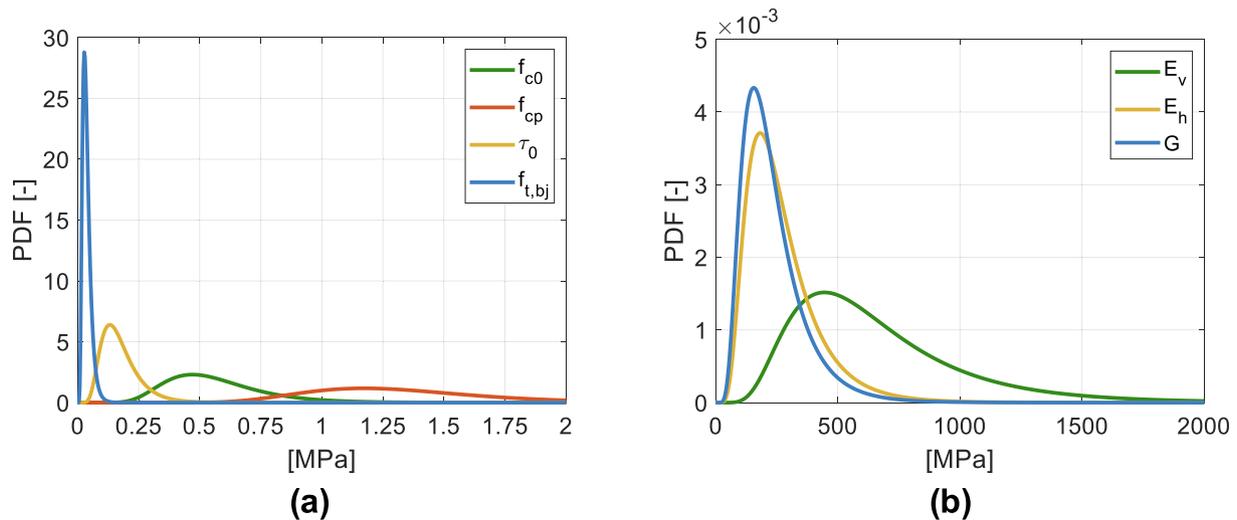
Fig. 10. Lognormal probability density functions (PDF) for (a) strength parameters, (b) stiffness parameters.

4. Discussion of the seismic fragility results

Fig. 11 shows an example of the derivation of DS# fragility for the UFB* building class. In particular, it refers to the IP damage mode, SPO2IDA assessment technique, and DS4. The grey lines represent the fragility curves of the portfolio of buildings where each curve is the maximum envelope of the façades' fragilities of a building. The solid red line represents the mean fragility at conditional PGA. The black lines (solid and dash-dotted) represent the mean $+/-$ standard deviation fragilities to illustrate the dispersion around the mean result. Lastly, the red dash-dotted line indicates the lognormal approximation of the mean fragility. For a given probability of exceedance, the dispersion around the mean estimate can be quantified with the formula reported in Section 2.3.1., $\beta = 0.5 \times \ln (\mathrm{PGA}_{84\%}/\mathrm{PGA}_{16\%})$. For instance, at $\mathrm{P}(\mathrm{D} \geq \mathrm{DS4}|\mathrm{PGA}) = 0.5$ (median value of the fragility curve), the dispersion β is equal to 0.55. This value indicates that the sources of inter-/intra-building variability introduced in the model adequately reflect the typical confidence interval of

fragility curves of portfolio of buildings (e.g. [80]).

The full set of mean fragility estimates is shown in Fig. 12, while the corresponding lognormal parameters (median η and lognormal standard deviation β) are summarised in Table 2. Fig. 12a-b shows the IP damage fragilities assessed with SPO2IDA and CSM, respectively. Fig. 12c-d includes the corresponding OOP fragility curves. Lastly, Fig. 12e-f depicts the average SPO2IDA-CSM fragility estimates. In addition, fragility curves for brick masonry buildings developed by GEM [13] and relevant to Malawi are plotted along with the IP estimates.

The key findings of the study are summarised as follow:

The IP fragility estimates (Fig. 12a-b-e) are characterised by a close similarity between the DS3 and DS4 curves. This can be explained by looking at the IP force–displacement response of the façades (example in Fig. 4d). In most cases, the post-peak response presents a rapid decay in horizontal capacity. Consequently, the DS4 displacement (defined at 80% post-peak capacity) is close to the displacement at peak horizontal capacity. In other words, the similarity between DS3 and DS4 is the result of the brittle IP response of the façades, as discussed in Section 2.1.1.

The OOP fragility curves (Fig. 12c-d-f) present lower median PGA values with respect to IP estimates. This is an expected result given the well-known vulnerability of non–engineered URMs against OOP loads [8,25]. Therefore, UFB* buildings are more likely to experience partial OOP failures of walls rather than widespread IP damage.

The comparison between CSM and SPO2IDA provides interesting insights on the epistemic uncertainty of seismic assessment methods. Looking at the IP damage mode, the CSM results are more conservative than SPO2IDA, in agreement with previous research findings [81]. In particular, median values of DS fragilities are approximately 20% lower for CSM with respect to SPO2IDA. Both techniques provide reasonable fragility results, therefore, to account for the epistemic uncertainty with regard to the seismic performance assessment, the mean IP fragilities (Fig. 12e) should be considered. In contrast, when looking at the OOP damage mode, the CSM η values are consistently higher than the corresponding SPO2IDA estimates
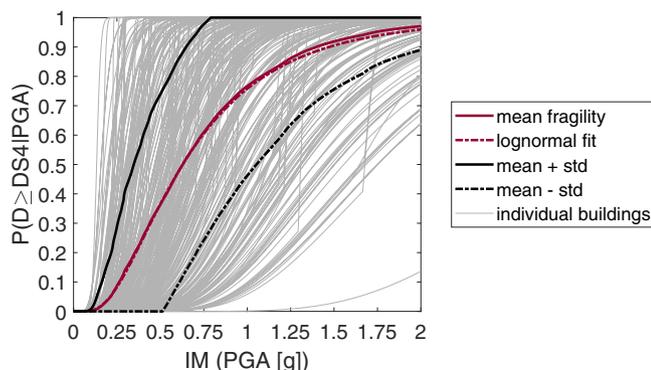
Fig. 11. Example of UFB* class fragility derivation (IP/SPO2IDA/DS4).
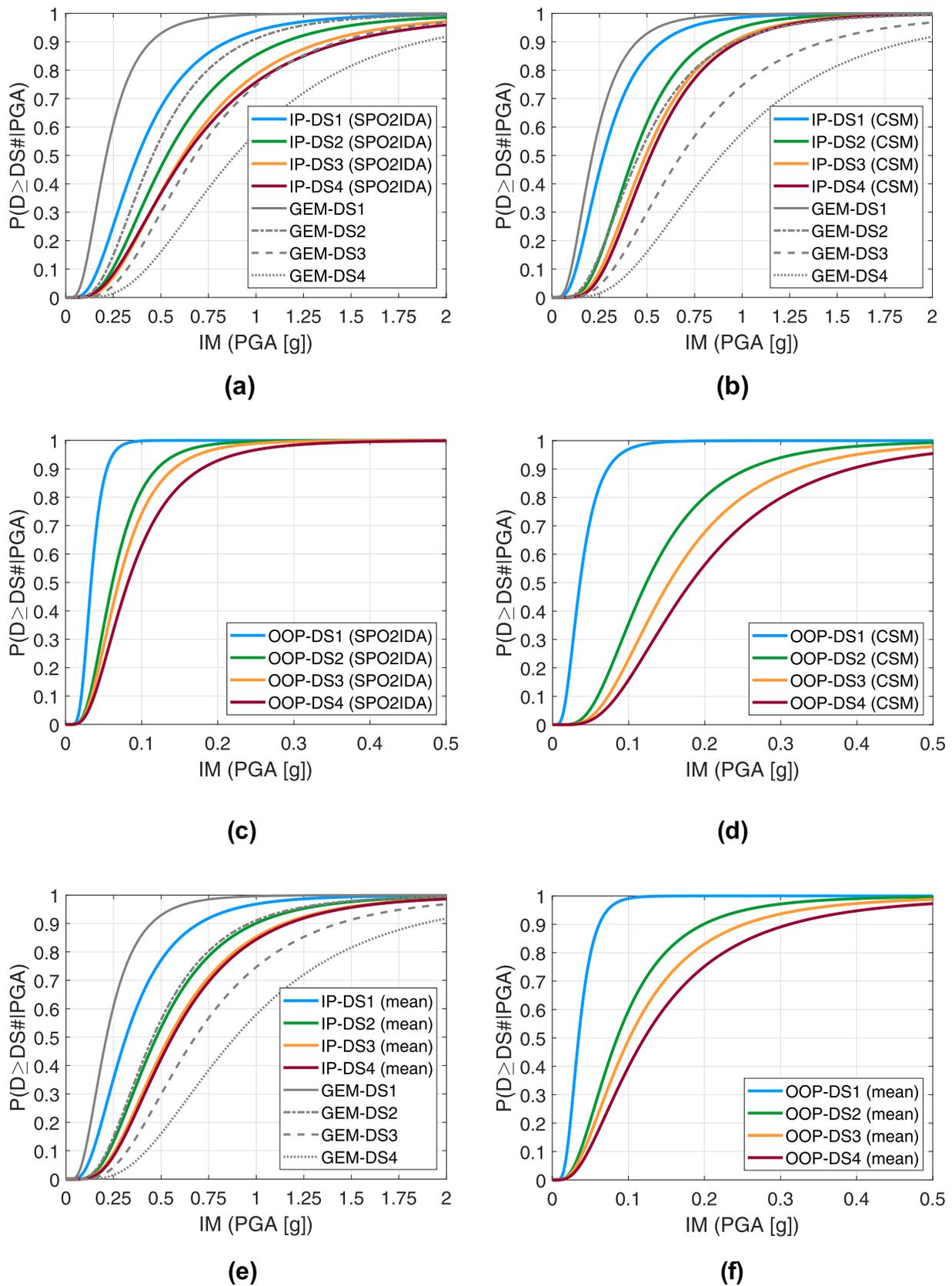
Fig. 12. Mean fragility curves for different damage mechanisms and assessment techniques: (a) IP-SPO2IDA, (b) IP-CSM, (c) OOP-SPO2IDA, (d) OOP-CSM, (e) IP-mean, (f) OOP-mean.

(about two times higher). More generally, the OOP-SPO2IDA fragilities seem too conservative with respect to experimental evidence [56] and previous research works on OOP fragility of URMs [25,28,29]. Meanwhile

the CSM fragilities are in line with the literature and should be selected to characterise the OOP vulnerability of the UFB* category.

Lastly, the comparison between the IP fragilities of this study and the

Table 2
Lognormal parameters of seismic fragility curves.

	DS1 (slight)		DS2 (moderate)		DS3 (extensive)		DS4 (near collapse)	
	η	β	η	β	η	β	η	B
IP (SPO2IDA)	0.38	0.63	0.53	0.60	0.61	0.62	0.63	0.66
IP (CSM)	0.27	0.59	0.43	0.50	0.49	0.51	0.52	0.50
OOP (SPO2IDA)	0.034	0.37	0.062	0.52	0.070	0.56	0.082	0.61
OOP (CSM)	0.036	0.54	0.12	0.57	0.15	0.58	0.18	0.60
IP (mean)	0.32	0.62	0.48	0.58	0.54	0.58	0.56	0.58
OOP (mean)	0.035	0.45	0.085	0.66	0.10	0.71	0.12	0.74
GEM [13]	0.21	0.58	0.46	0.58	0.68	0.58	0.89	0.58

ones of GEM (Martins and Silva [13]) displays a satisfactory match on the median values and a very good fitting of the dispersions β. In particular, the GEM fragilities provide larger median estimates with respect to the results of this work since: (i) they have been derived with nonlinear time history analysis on equivalent SDOFs (a less conservative technique with respect to nonlinear static analysis/simplified IDA), and (ii) the nonlinear response of the equivalent SDOF is quantified by assuming a global response of the URM building.

5. Conclusions

The fragility model presented in this paper refers to typical URM brick-in-cement houses in Malawi. The work merges research findings on structural materials and in-field data on building geometries. This allows the estimation of new country-specific fragility curves, currently not available in the technical-scientific literature. The procedure adopted to derive fragility curves provides estimates for in-plane and out-of-plane damage potential. The epistemic uncertainty around seismic assessment methods is also addressed by using two established approaches, the CSM and SPO2IDA. The key finding of the study is that non-engineered Malawian houses are highly vulnerable to out-of-plane damage, something that could be prevented by improving construction details such as wall-to-wall and wall-to-roof connections. If out-of-plane action is controlled, masonry walls are more likely to sustain in-plane damage first. In general, the fragility of Malawian URMs appears larger than the estimate provided by global models. In risk analyses, it is suggested to adopt IP-mean fragility sets (Fig. 12e) for buildings with good construction details and OOP-CSM fragilities (Fig. 12d) for low-quality buildings. In conclusion, the new fragility curves represent a consistent advancement towards the implementation of earthquake risk modelling studies in the context of Malawi and in the wider East African region.

6. Data access statement

The underlying data for this study were drawn from the referenced literature. All the data produced in this work are provided in full within this paper.

Declaration of Competing Interest

The authors declare that they have no known competing financial interests or personal relationships that could have appeared to influence the work reported in this paper.

References

[1] United Nations Department of Economic and Social Affairs Population Division. World Population Prospects 2019: Data Booket. ST/ESA SER.A/424. 2019.

[2] Mwale FD, Adeloye AJ, Beevers L. Quantifying vulnerability of rural communities to flooding in SSA: a contemporary disaster management perspective applied to the Lower Shire Valley, Malawi. Int J Disaster Risk Reduct 2015;12:172–87. https://doi.org/10.1016/j.ijdrr.2015.01.003.

[3] Manda M, Wanda E. Understanding the nature and scale of risks in Karonga, Malawi. Environ Urban 2017;29(1):15–32. https://doi.org/10.1177/0956247817692200.

[4] Kita SM. Barriers or enablers? Chiefs, elite capture, disasters, and resettlement in rural Malawi. Disasters 2019;43(1):135–56. https://doi.org/10.1111/disa:2019.43.issue-110.1111/disa:12295.

[5] Mawenda J, Watanabe T, Avtar R. An Analysis of Urban Land Use/Land Cover Changes in Blantyre City, Southern Malawi (1994–2018). Sustainability 2020;12:2377. https://doi.org/10.3390/su12062377.

[6] De Risi R, De Paola F, Turpie J, Kroeger T. Life Cycle Cost and Return on Investment as complementary decision variables for urban flood risk management in developing countries. Int J Disaster Risk Reduct 2018;28:88–106. https://doi.org/10.1016/j.ijdrr.2018.02.026.

[7] Goda K, Gibson ED, Smith HR, Biggs J, Hodge M. Seismic risk assessment of urban and rural settlements around Lake Malawi. Front Built Environ 2016. https://doi.org/10.3389/fbuil.2016.00030.

[8] World Bank, Malawi Government. Safer School Construction Guidelines - Technical Manual. 2019.

[9] Hodge M, Biggs J, Goda K, Aspinall W. Assessing infrequent large earthquakes using geomorphology and geodesy: the Malawi Rift. Nat Hazards 2015;76(3):1781–806. https://doi.org/10.1007/s11069-014-1572-y.

[10] Jaiswal K, Wald D, D'Ayala D. Developing empirical collapse fragility functions for global building types. Earthq Spectra 2011;27(3):775–95. https://doi.org/10.1193/1.3606398.

[11] So E, Spence R. Estimating shaking-induced casualties and building damage for global earthquake events: a proposed modelling approach. Bull Earthq Eng 2013;11(1):347–63. https://doi.org/10.1007/s10518-012-9373-8.

[12] Kloukinas P, Novelli V, Kafodya I, Ngoma I, Macdonald J, Goda K. A building classification scheme of housing stock in Malawi for earthquake risk assessment. J Hous Built Environ 2020;35(2):507–37. https://doi.org/10.1007/s10901-019-09697-5.

[13] Martins L, Silva V. Development of a fragility and vulnerability model for global seismic risk analyses. Bull Earthq Eng 2020:in review. doi:10.1007/s10518-020-00885-1.

[14] Pagani M, Garcia-Pelaez J, Gee R, Johnson K, Poggi V, Silva V, et al. The 2018 version of the Global Earthquake Model: Hazard component. Earthq Spectra 2020;36(1_suppl):226–51. https://doi.org/10.1177/8755293020931866.

[15] Modelling Exposure Through Earth Observation Routines (METEOR) 2020. https://meteor-project.org/data.

[16] Novelli VI, De Risi R, Ngoma I, Kafodya I, Kloukinas P, Macdonald J, et al. Fragility curves for non-engineered masonry buildings in developing countries derived from real data based on structural surveys and laboratory tests. Soft Comput 2021;25(8):6113–38. https://doi.org/10.1007/s00500-021-05603-w.

[17] D'Ayala D, Speranza E. Definition of collapse mechanisms and seismic vulnerability of historic masonry buildings. Earthq Spectra 2003;19(3):479–509. https://doi.org/10.1193/1.1599896.

[18] Novelli V, Kloukinas P, Ngoma I, Kafodya I, Macdonald J, Goda K. Unreinforced masonry houses made of fired clay bricks (Malawi) - Report#205. 2018.

[19] Kloukinas P, Kafodya I, Ngoma I, Novelli V, Macdonald J, Goda K. Strength of materials and masonry structures in Malawi. 7th Int. Conf. Struct. Eng. Mech. Comput., Cape Town, South Africa: CRC press; 2019.

[20] Voyagaki E, Kloukinas P, Novelli V, De Risi R, Kafodya I, Ngoma I, et al. Masonry Panel Testing in Malawi. 17th World Conf. Earthq. Eng., Sendai, Japan: 2020.

[21] Giordano N, De Luca F, Sextos A. Out-of-plane closed-form solution for the seismic assessment of unreinforced masonry schools in Nepal. Eng Struct 2020;203:109548. https://doi.org/10.1016/j.engstruct.2019.109548.

[22] Vamvatsikos D, Allin Cornell C. Direct estimation of the seismic demand and capacity of oscillators with multi-linear static pushovers through IDA. Earthq Eng Struct Dyn 2006;35(9):1097–117. https://doi.org/10.1002/(ISSN)1096-984510.1002/eqe.v35:910.1002/eqe.573.

[23] Freeman SA. Prediction of response of concrete buildings to severe earthquake motion. ACI J 1978;55:589–606. https://doi.org/10.14359/6629.

[24] Lagomarsino S. Seismic assessment of rocking masonry structures. Bull Earthq Eng 2015;13(1):97–128. https://doi.org/10.1007/s10518-014-9609-x.

[25] Giordano N, De Luca F, Sextos A. Analytical fragility curves for masonry school building portfolios in Nepal. Bull Earthq Eng 2021;19(2):1121–50. https://doi.org/10.1007/s10518-020-00989-8.

[26] Lourenço PB, Mendes N, Ramos LF, Oliveira DV. Analysis of masonry structures without box behavior. Int J Archit Herit 2011;5(4-5):369–82. https://doi.org/10.1080/15583058.2010.528824.

[27] Jalayer F, Carozza S, De Risi R, Manfredi G, Mbuya E. Performance-based flood safety-checking for non-engineered masonry structures. Eng Struct 2016;106:109–23. https://doi.org/10.1016/j.engstruct.2015.10.007.

[28] Borzi B, Crowley H, Pinho R. Simplified pushover-based earthquake loss assessment (SP-BELA) method for masonry buildings. Int J Archit Herit 2008;2(4):353–76. https://doi.org/10.1080/15583050701828178.

[29] Ceran HB, Erberik MA. Effect of out-of-plane behavior on seismic fragility of masonry buildings in Turkey. Bull Earthq Eng 2013;11(5):1775–95. https://doi.org/10.1007/s10518-013-9449-0.

[30] PEER Pacific Earthquake Engineering Research Center. OpenSees: Open system for earthquake engineering simulation 2000.

[31] Petracca M, Candeloro F, Camata G. STKO Scientific ToolKit for OpenSees - STKO user manual 2017.

[32] De Luca F, Vamvatsikos D, Iervolino I. Near-optimal piecewise linear fits of static pushover capacity curves for equivalent SDOF analysis. Earthq Eng Struct Dyn 2013;42(4):523–43. https://doi.org/10.1002/eqe.v42.410.1002/eqe.2225.

[33] Lagomarsino S, Cattari S. PERPETUATE guidelines for seismic performance-based assessment of cultural heritage masonry structures. Bull Earthq Eng 2015;13(1):13–47. https://doi.org/10.1007/s10518-014-9674-1.

[34] Roca P, Molins C, Marí AR. Strength capacity of masonry wall structures by the equivalent frame method. J Struct Eng 2005;131(10):1601–10. https://doi.org/10.1061/(ASCE)0733-9445(2005)131:10(1601).

[35] Lagomarsino S, Penna A, Galasco A, Cattari S. TREMURI program: an equivalent frame model for the nonlinear seismic analysis of masonry buildings. Eng Struct 2013;56:1787–99. https://doi.org/10.1016/j.engstruct.2013.08.002.

[36] Giordano N, Mosalam KM, Günay S. Probabilistic performance-based seismic assessment of an existing masonry building. Earthq Spectra 2020;36(1):271–98. https://doi.org/10.1177/8755293019878191.

[37] Simões A, Milošević J, Meireles H, Bento R, Cattari S, Lagomarsino S. Fragility curves for old masonry building types in Lisbon. Bull Earthq Eng 2015;13(10):3083–105. https://doi.org/10.1007/s10518-015-9750-1.

[38] Rota M, Penna A, Magenes G. A methodology for deriving analytical fragility curves for masonry buildings based on stochastic nonlinear analyses. Eng Struct 2010;32(5):1312–23. https://doi.org/10.1016/j.engstruct.2010.01.009.

[39] Quagliarini E, Maracchini G, Clementi F. Uses and limits of the Equivalent Frame Model on existing unreinforced masonry buildings for assessing their seismic risk: a review. J Build Eng 2017;10:166–82. https://doi.org/10.1016/j.jobe.2017.03.004.

[40] Bracchi S, Rota M, Penna A, Magenes G. Consideration of modelling uncertainties in the seismic assessment of masonry buildings by equivalent-frame approach. Bull Earthq Eng 2015;13(11):3423–48. https://doi.org/10.1007/s10518-015-9760-z.

[41] Lourenço PB, Milani G, Tralli A, Zucchini A. Analysis of masonry structures: review of and recent trends in homogenization techniques. Can J Civ Eng 2007;34:1443–57. https://doi.org/10.1139/L07-097.

[42] Lourenço PB, Rots JG, Blaauwendraad J. Continuum model for masonry: parameter estimation and validation. J Struct Eng 1998;124(6):642–52. https://doi.org/10.1061/(ASCE)0733-9445(1998)124:6(642).

[43] Pelà L, Cervera M, Roca P. An orthotropic damage model for the analysis of masonry structures. Constr Build Mater 2013;41:957–67. https://doi.org/10.1016/j.conbuildmat.2012.07.014.

[44] Calderini C, Lagomarsino S. Continuum model for in-plane anisotropic inelastic behavior of masonry. J Struct Eng 2008;134(2):209–20. https://doi.org/10.1061/(ASCE)0733-9445(2008)134:2(209).

[45] Petracca M, Pelà L, Rossi R, Zaghi S, Camata G, Spacone E. Micro-scale continuous and discrete numerical models for nonlinear analysis of masonry shear walls. Constr Build Mater 2017;149:296–314. https://doi.org/10.1016/j.conbuildmat.2017.05.130.

[46] Petracca M, Pelà L, Rossi R, Oller S, Camata G, Spacone E. Regularization of first order computational homogenization for multiscale analysis of masonry structures. Comput Mech 2016;57(2):257–76. https://doi.org/10.1007/s00466-015-1230-6.

[47] Roca P, Cervera M, Pelà L, Clemente R, Chiumenti M. Continuum FE models for the analysis of Mallorca Cathedral. Eng Struct 2013;46:653–70. https://doi.org/10.1016/j.engstruct.2012.08.005.

[48] Lourenço PB, Krakowiak KJ, Fernandes FM, Ramos LF. Failure analysis of Monastery of Jeronimos, Lisbon: How to learn from sophisticated numerical models. Eng Fail Anal 2007;14:280–300. https://doi.org/10.1016/j.engfailanal.2006.02.002.

[49] Silva LC, Mendes N, Lourenço PB, Ingham J. Seismic Structural Assessment of the Christchurch Catholic Basilica, New Zealand. Structures 2018;15:115–30. https://doi.org/10.1016/j.istruc.2018.06.004.

[50] Novelli VI, D'Ayala D, Makhloufi N, Benouar D, Zekagh A. A procedure for the identification of the seismic vulnerability at territorial scale. Application to the Casbah of Algiers. Bull Earthq Eng 2015;13(1):177–202. https://doi.org/10.1007/s10518-014-9666-1.

[51] Petracca M, Camata G. A Mixed Implicit-Explicit Tension-Compression Plastic-Damage Model. Pescara, Italy: 2019.

[52] European Commitee for Standardization Eurocode 8: Design of structures for earthquake resistance - Part 1: General rules, seismic actions and rules for buildings Eur Comm Stand 1 2004 231 [Authority: The European Union per Regulation 305/2011, Directive 98/34/EC, Directive 2004/18/EC].

[53] Foraboschi P. Coupling effect between masonry spandrels and piers. Mater Struct 2009;42(3):279–300. https://doi.org/10.1617/s11527-008-9405-7.

[54] Shahzada K, Khan AN, Elnashai AS, Ashraf M, Javed M, Naseer A, et al. Experimental seismic performance evaluation of unreinforced brick masonry buildings. Earthq Spectra 2012;28(3):1269–90. https://doi.org/10.1193/1.4000073.

[55] Griffith MC, Lam NTK, Wilson JL, Doherty K. Experimental investigation of unreinforced brick masonry walls in flexure. J Struct Eng 2004;130(3):423–32. https://doi.org/10.1061/(ASCE)0733-9445(2004)130:3(423).

[56] Shawa OA, Felice G, Mauro A, Sorrentino L. Out-of-plane seismic behaviour of rocking masonry walls. Earthq Eng Struct Dyn 2012;41(5):949–68. https://doi.org/10.1002/eqe.v41.510.1002/eqe.1168.

[57] Ferreira TM, Costa AA, Costa A. Analysis of the out-of-plane seismic behavior of unreinforced masonry: a literature review. Int J Archit Herit 2015;9(8):949–72. https://doi.org/10.1080/15583058.2014.885996.

[58] Degli Abbati S, Lagomarsino S. Out-of-plane static and dynamic response of masonry panels. Eng Struct 2017;150:803–20. https://doi.org/10.1016/j.engstruct.2017.07.070.

[59] Manandhar V, Shrestha H, Marasini N, Prajapati R, Guragain R, Chaulagain R, et al. Experimental investigation of low cost steel wire mesh retrofit for stonemasonry in mud mortar. 17th World Conf Earthq. Eng., Sendai; 2020.

[60] Giordano N, Crespi P, Franchi A. Flexural strength-ductility assessment of unreinforced masonry cross-sections: analytical expressions. Eng Struct 2017;148:399–409. https://doi.org/10.1016/j.engstruct.2017.06.047.

[61] Erberik MA. Generation of fragility curves for Turkish masonry buildings considering in-plane failure modes. Earthq Eng Struct Dyn 2008;37(3):387–405. https://doi.org/10.1002/(ISSN)1096-984510.1002/eqe.v37:310.1002/eqe.760.

[62] Silva V, Akkar S, Baker J, Bazzurro P, Castro JM, Crowley H, et al. Current challenges and future trends in analytical fragility and vulnerability modeling. Earthq Spectra 2019;35(4):1927–52. https://doi.org/10.1193/042418EQS101O.

[63] Boore DM, Stewart JP, Seyhan E, Atkinson GM. NGA-West2 equations for predicting PGA, PGV, and 5% damped PSA for shallow crustal earthquakes. Earthq Spectra 2014;30(3):1057–85. https://doi.org/10.1193/070113EQS184M.

[64] Wald DJ, Allen TI. Topographic slope as a proxy for seismic site conditions and amplification. Bull Seismol Soc Am 2007;97(5):1379–95. https://doi.org/10.1785/0120060267.

[65] Malhotra PK. Smooth spectra of horizontal and vertical ground motions. Bull Seismol Soc Am 2006;96(2):506–18. https://doi.org/10.1785/0120050062.

[66] Smerzini C, Galasso C, Iervolino I, Paolucci R. Ground motion record selection based on broadband spectral compatibility. Earthq Spectra 2014;30(4):1427–48. https://doi.org/10.1193/052312EQS197M.

[67] Bommer JJ, Acevedo AB. The use of real earthquake accelerograms as input to dynamic analysis. J Earthq Eng 2004;8:43–91. doi:10.1080/13632460409350521.

[68] European Commitee for Standardization. EN 1052-1:1999 - Methods of test for masonry - Part 1: Determination of compressive strength. Brussels, Belgium: 1999.

[69] Malawi Bureau of Standards. MS791-1. The structural use of masonry – Code of practice, Part 1: Unreinforced masonry walling. 2014.

[70] Bureau TNM. Safer House Construction Guidelines. 2016.

[71] Brignola A, Frumento S, Lagomarsino S, Podestà S. Identification of Shear Parameters of Masonry Panels Through the In-Situ Diagonal Compression Test. Int J Archit Herit 2008;3(1):52–73. https://doi.org/10.1080/15583050802138634.

[72] Malawi Bureau of Standards. MS6 - Burnt bricks specification. Blantyre, Malawi: 1994.

[73] Kaushik HB, Rai DC, Jain SK. Stress-strain characteristics of clay brick masonry under uniaxial compression. J Mater Civ Eng 2007;19(9):728–39. https://doi.org/10.1061/(ASCE)0899-1561(2007)19:9(728).

[74] European Commitee for Standardization. EN 1052-2:1999 - Methods of test for masonry - Part 2: Determination of flexural strength. Brussels, Belgium: 1999.

[75] Mojsilovic N. A discussion of masonry characteristics derived from compression tests. 10th Can. Mason. Symp., Banff, Canada: 2005.

[76] Wilding BV, Godio M, Beyer K. The ratio of shear to elastic modulus of in-plane loaded masonry. Mater Struct 2020;53:40. https://doi.org/10.1617/s11527-020-01464-1.

[77] Facconi L, Minelli F, Lucchini S, Plizzari G. Experimental study of solid and hollow clay brick masonry walls retrofitted by steel fiber-reinforced mortar coating. J Earthq Eng 2020;24(3):381–402. https://doi.org/10.1080/13632469.2018.1442264.

[78] Augenti N, Parisi F, Acconcia A. MADA Online experimental database for mechanical modelling of existing masonry assemblages. Proc 15th World Conf Earthq Eng 2012.

[79] da Porto F, Guidi G, Garbin E, Modena C. In-plane behavior of clay masonry walls: experimental testing and finite-element modeling. J Struct Eng 2010;136(11):1379–92. https://doi.org/10.1061/(ASCE)ST.1943-541X.0000236.

[80] Jalayer F, De Risi R, Manfredi G. Bayesian Cloud Analysis: efficient structural fragility assessment using linear regression. Bull Earthq Eng 2015;13(4):1183–203. https://doi.org/10.1007/s10518-014-9692-z.

[81] Vargas YF, Pujades LG, Barbat AH, Hurtado JE. Incremental Dynamic Analysis and Pushover Analysis of Buildings. A Probabilistic Comparison. In: Papadrakakis M, Stefanou G, Papadopoulos V, editors., Dordrecht: Springer Netherlands; 2013, p. 293–308. doi:10.1007/978-94-007-5134-7_17.